Chapter 6

Cohesion

6.1 Introduction

One of the salient properties of solids is that they adopt well ordered crystalline structures with well defined lattice constants at low enough temperatures. Having discussed the many-body Hamiltonian of a solid and its calculation in some detail in the previous chapters, it is natural to ask in how much this helps us already to understand why a given element chooses a particular crystal structure and what kind of properties are connected with it. This topic is called cohesion, and we need to examine the nature of chemical bonding in solids to understand their cohesive properties.
Just like in all previous chapters, we will restrict ourselves to the situation $T \approx 0$, viz. sufficiently low temperatures. This is because at higher temperatures, the properties of matter do not only follow from the total energy, but are also governed by other free energy contributions. Differing vibrational properties of different crystalline structures can induce structural phase transitions to other configurations upon heating, and, in fact most elements switch their crystal structure several times before they melt. Another thing is that we would need to worry about the contribution from the configurational entropy e.g. of defects. At low enough temperatures, however, the cohesive properties follow predominantly from the chemical binding in a perfect lattice, i.e. from the electrostatic interaction of the electron density with the ions and the ion-ion interaction. And this is what we want to study in this chapter.
The central property of low temperature cohesion is the *cohesive energy* E^{coh}, which is the energy needed in order to rip a sample apart into a gas of widely separated atoms. If $\{\mathbf{R}\}$ denotes a set of structural parameters characteristic for a crystal lattice, and $\{\mathbf{R_o}\}$ represents their value at the equilibrium crystal structure (neglecting zero-point vibrations), we thus have

$$E^{\mathrm{coh}} \;=\; -\left(\frac{E(\{\mathbf{R_o}\})}{M} - \frac{E(\{\mathbf{R}\}\to\infty)}{M}\right). \tag{6.1}$$

Here E is the total energy of the solid (< 0), and M the number of atoms in the crystal. Note that with this definition, the cohesive energy is a positive number. More generally, one could also say that the cohesive energy is the energy required to separate a solid into its elementary "building blocks". It is usually understood that these "building blocks" are the neutral atoms, but sometimes it can be more convenient to use molecules (e.g. N_2 for solid nitrogen) or ions (e.g. Na^+ and Cl^- for NaCl). By an appropriate correction

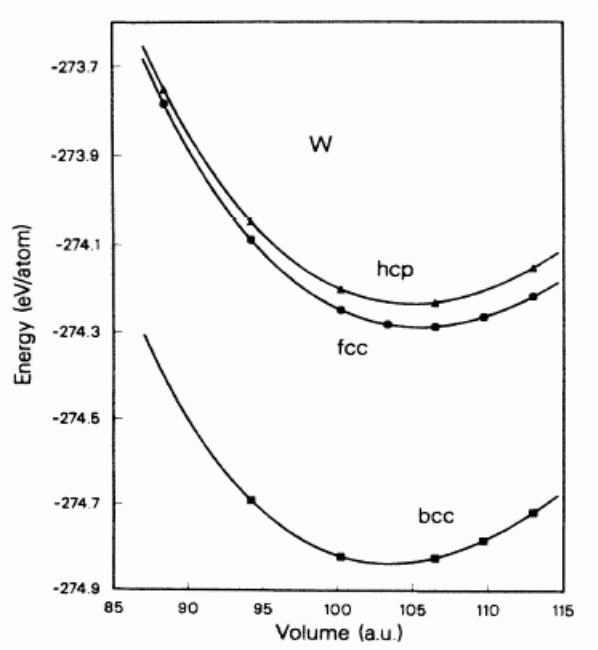

Figure 6.1: DFT-LDA total energy versus volume for W in the fcc, hcp and bcc structure [from C.T. Chan *et al.*, Phys. Rev. B **33**, 7941 (1986)].

for the molecular dissociation energy, or the ionization energy of the cation (energy to remove an electron) and the electron affinity of the anion (energy to add an electron), such numbers can always be translated into the cohesive energy with respect to neutral atoms, which is what we will use primarily.

By itself, the cohesive energy does not have much significance. It is not easy to measure experimentally, and it bears no relation to the practical strengths of solids. Practical strength is rather governed by resistance to flow and fracture, which are physically quite distinct from cohesive energy. The question that cohesive energy makes possible to answer, on the other hand, is which crystal structure the solid will adopt, namely the one with the highest E^{coh} (which is nothing else but the system achieving its lowest total energy). With the electronic structure methods discussed in the preceding chapters, the straightforward approach to cohesion would therefore simply be to compute the total energy of the crystal as a function of $\{\mathbf{R}\}$ for a given lattice structure. The energy lowering obtained at the minimum $\{\mathbf{R_o}\}$ gives then the cohesive energy achievable in this particular lattice structure (cf. also with Fig. 2 of chapter 1). Repating this for all sorts of lattices would finally help us to identify the one which yields the highest E^{coh} and this will be the equilibrium crystal structure at low temperatures.

Fig. 6.1 shows how this works in practice. Here, the total energy of tungsten has been computed with density-functional theory (DFT-LDA) as a function of the unit-cell volume V (i.e. using this one variable to represent the set $\{\mathbf{R}\}$ for these high symmetry structures). The points are the actually calculated values for the fcc, the hcp and the bcc crystal structure. In order to obtain reliable minimum values for these discrete sets of points (and also to reduce the inherent numerical noise), one usually interpolates the obtained curves with so-called *equation of state* functions, which are analytical functions

derived from general thermodynamic considerations about the internal energy in the vicinity of the minimum. A popular form is the equation due to Murnaghan (F.D. Murnaghan, Proc. Natl. Acad. Sci. U.S.A. **30**, 244 (1944)),

$$\frac{E(V)}{M} - \frac{E(V_o)}{M} = \frac{B_o V}{B_o'(B_o'-1)}\left[B_o'\left(1-\frac{V_o}{V}\right) + \left(\frac{V_o}{V}\right)^{B_o'} - 1\right] \quad , \tag{6.2}$$

which involves the following quantities

V_o: Volume at the energy minimum

B_o: Bulk modulus at V_o, as already defined in chapter 1. $B_o = V\frac{\partial^2 E(V)}{\partial V^2}\Big|_{V=V_o}$

B_o': $= \frac{\partial B}{\partial p}\Big|_{V=V_o}$

Fitting V_o, B_o and B_o' to the DFT data, the solid curves in Fig. 6.1 are obtained. We see that over quite a range of volumes this fit is perfect. In this particular case, the bcc structure is correctly obtained as ground state crystal structure of W, with an equilibrium lattice constant $a_o = (2V_o)^{\frac{1}{3}} = 3.13\,\text{Å}$ and a bulk modulus $B_o = 3.33\,\text{Mbar}$, which compare very well to the experimental values of 3.16 Å and 3.23 Mbar, respectively. Also, the agreement of the derived $E^{\text{coh}} = 9.79\,\text{eV}$ (exp: 8.90 eV) with experiment is quite reasonable. In fact, the significant overbinding obtained (too high cohesive energy and slightly too short bond length) is typical for the employed LDA functional, and partially corrected in present day GGA functionals. Note also, that less symmetric structures with a more atom basis often require a more extended set of $\{\mathbf{R}\}$ than just one parameter. One then has to compute the total energy as a higher dimensional function, e.g. of a and c (in plane and out of plane lattice constant) for the hcp structure.
A similarly precise description of the cohesive properties as obtained for tungsten can be achieved by present day DFT calculations for most elemental and compound solids. With this, we could in principle already close the chapter on cohesion at this very moment. The level of accuracy we have achieved in describing the electronic interactions in solids seems enough to also fully explain the ensuing cohesive properties. Yet, although it is quite gratifying to have reached such a high degree of quantitative modeling with nowadays routinely employed electronic structure theories, this would still leave us somewhat unsatisfied. Because what we have not yet gained is an *understanding* of *why* the bcc structure is actually the most favored one for W, and *why* the cohesive energy has roughly the value it has. Even more important, we would also like to understand, why the cohesive energy and equilibrium crystal structure exhibit certain trends over the periodic system of elements as exemplified in Fig. 6.2.
Such an understanding has historically been developed by discussing four idealized types of bonding: *van der Waals, ionic, covalent* and *metallic*. Almost no real solid can be classified 100% into any one of these four categories, but it has proven useful to look at these extremes, to understand and describe the largely varying cohesive properties of solids. Intimately connected with this is the desire to motivate and obtain so-called *interatomic potentials* for solids. In order to quickly obtain the total energy of a solid in any arbitrary geometrical configuration, the ultimate goal of material scientists is to find such potentials, which give the total energy as just an analytic function of the specified atomic positions (and distances) in the solid. Such potentials would correspondingly

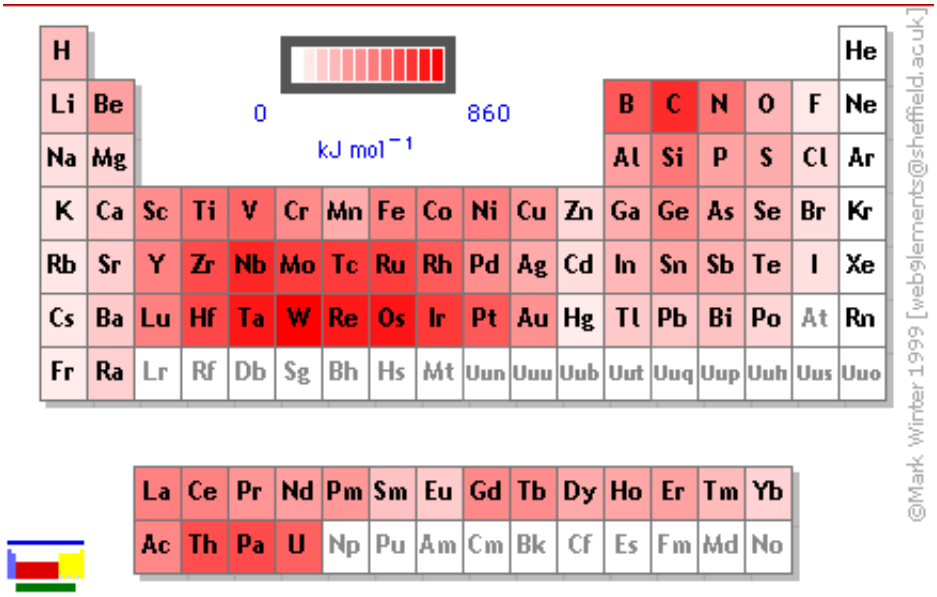

Figure 6.2: Experimental cohesive energy over the periodic system of elements (96 kJ/mole = 1 eV). [From Webelements].

make the explicit, time-consuming quantum-mechanical calculation of the many-body Hamiltonian for each new atomic configuration obsolete; the results would already be condensed in the particular functional form of the employed interatomic potential. In the modern multi-scale modeling language this is called *coarse graining out the electronic degrees of freedom*. This endeavor has been met with varying success for solids belonging to the four bonding categories, and discussing them in more detail we will see why or why not this approach fails, viz. what general properties such interatomic potentials would need to have.

6.2 Van der Waals Bonding

The classical elements connected to the concept of van der Waals bonding are the rare gas atoms Ne, Ar, Kr, Xe (leaving out He with its extremely light mass, which exhibits special properties due to ensuing strong quantum-mechanical effects/zero-point vibrations). Fig. 6.3 illustrates the conceptual idea of this bonding using the example of two neon atoms. Noble metals have filled shells, and there is a rather large energy gap to the lowest lying unoccupied states in the next shell. As soon as the wave functions of the two neon atoms start to overlap, electrons would need to go to these much higher states, since there are no free states in the shell left and the Pauli principle forbids two electrons in the same states (technically the wave functions need to orthogonalize, yielding new solutions with high energy). This occupation of high lying states costs a lot of energy, the total energy goes up, or in other words we have a strongly repulsive interaction. Obviously, this so-called *Pauli repulsion* (or *hard core repulsion*) will always occur, when filled shells start to overlap significantly. Ultimately, it is thus the mechanism responsible for the steep increase of the total energy in all bonding types at very small distances (as soon as the inner shells of

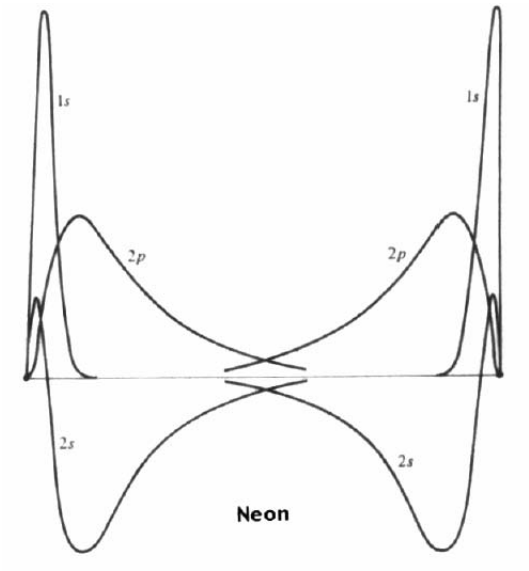

Figure 6.3: Radial atomic wave functions of two neon atoms at the equilibrium interatomic distance. Since the distance is relatively large, there is hardly any overlap of the wavefunctions [from Ashcroft and Mermin].

the atoms start to overlap). The big difference with the noble metals is that this happens already at relatively large distances, when the valence shells start to overlap, thereby preventing a closer approach of the two atoms. That there is an attractive interaction at all in this case is only due to small quantum mechanical fluctuations in the electron density of any of the two atoms. These give rise to momentarily existing dipoles, and although they average out over time, instantaneous electric fields are produced by them at any moment in time, inducing corresponding dipoles on the other atom. The interaction then results from the (minute) attraction between these two fluctuating dipoles.
Qualitatively we would therefore expect a variation of the total energy of the two atoms with distance r as shown in Fig. 6.4. At large distances there is a weak attraction and at small distances there is a strong repulsion, giving rise to a weak bonding minimum in between. For the attractive part, we can even derive the rough functional form based on the above sketched understanding of interacting dipoles: The electric field connected to a dipole of dipole moment $\mathbf{P_1}$ is $\mathbf{E} \propto \frac{\mathbf{P_1}}{r^3}$. This field induces the dipole moment $\mathbf{P_2} = \alpha\mathbf{E} \simeq \alpha\frac{\mathbf{P_1}}{r^3}$ on the other atom, where α is the polarizability of the atom. The two dipoles $\mathbf{P_1}$ and $\mathbf{P_2}$ have then an interaction energy given by

$$\frac{\mathbf{P_1}\mathbf{P_2}}{r^3} \sim \frac{\alpha\mathbf{P_1}^2}{r^6} \quad , \tag{6.3}$$

i.e. we would roughly expect the attractive part to scale as $\sim -Ar^{-6}$, where A is a proportionality constant, and the negative sign indicates attraction.
Concerning the repulsive part due to the overlap of wavefunctions, an appealing choice for a functional form would be an exponentially increasing term (since atomic wavefunctions have exponentially decaying tails). However, historically a positive power law term $\sim Br^{-12}$ is rather used instead, leading in total to the so-called *Lennard-Jones 6-12 potential*

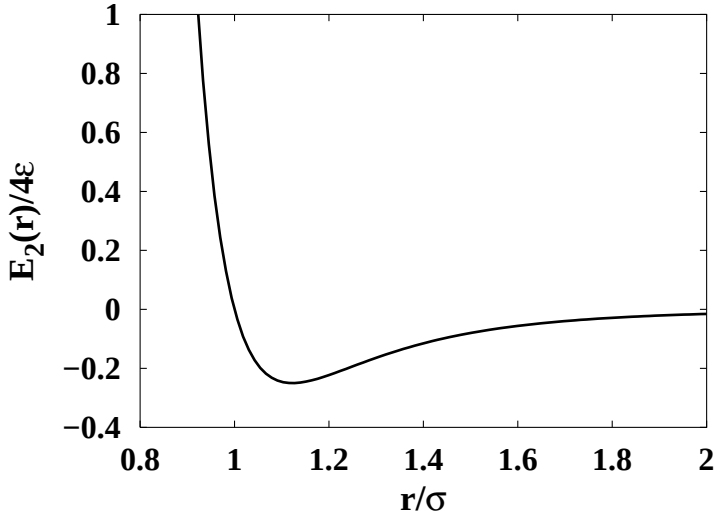

Figure 6.4: Lennard-Jones potential, cf. eq. (6.4), for the pair interaction between two rare gas atoms at distance r.

shown in Fig. 6.4. Using the units $\sigma = (B/A)^{1/6}$ and $\varepsilon = A^2/4B$, its functional form is typically written in a normalized way as

$$E_2^{\mathrm{LJ}}(r) \;=\; 4\varepsilon \left\{ \left(\frac{\sigma}{r}\right)^{12} \;-\; \left(\frac{\sigma}{r}\right)^{6} \right\} \quad . \tag{6.4}$$

The precise form of the repulsive term is in fact not even that important. Any term with an inverse power higher than 6 would have equally done to yield a steeply rising energy at small distances. And as a note aside, there are in fact other frequently employed potential forms like the Born-Meyer potential that use an exponential for the hard-core repulsion. With the Lennard-Jones potential, the complete interaction between two noble gas atoms is described by just two parameters (σ and ε). These can be obtained by fitting this curve either to experimental data from low density gases (second virial coefficient) or to computed total energy curves from highest order quantum chemistry approaches. Both yield virtually identical results, which can be almost perfectly fitted by the functional form of the Lennard-Jones curve. For Ne_2 one obtains e.g. $\sigma = 2.74\,\text{Å}$ and $\varepsilon = 3.1\,\text{meV}$ [cf. e.g. N. Bernardes, Phys. Rev. **112**, 1534 (1958)]. It is worth pointing out, however, that the current workhorse in electronic structure theory calculations, DFT, has some problems with such very weakly binding van der Waals systems. This is ultimately connected with that the presently employed functionals (like LDA or GGAs) contain only local exchange and correlation effects by construction. The dipole-dipole fluctuations responsible for the attractive part of the Lennard-Jones curve are, on the other hand, non-local in nature. This problem is usually simply summarized by saying that the current implementations of DFT cannot address van der Waals (or dispersion) forces. The actual state of the situation is nicely explained in Fig. 6.5, again for the Ne_2 molecule. Why LDA (or to a better degree GGAs with exact exchange admixture) nevertheless give a bonding minimum is still controversially discussed.

Having understood the binding between two noble gas atoms, a straightforward way of

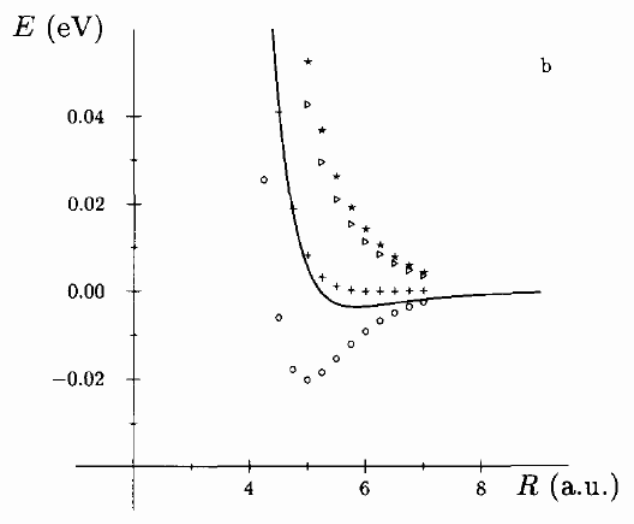

Figure 6.5: Total energy curve for the Ne_2 molecule. The solid line is the result from an "exact" highest-order quantum chemistry calculation, exhibiting the correct shallow binding minimum. DFT-LDA (circles), on the other hand, significantly overestimates this binding, whereas the GGA (stars) gives a purely repulsive curve. The admixture of exact exchange to the GGA (crosses) gives results that are not too far off anymore [from J.M. Perez-Jorda and A.D. Becke, Chem. Phys. Lett. **233**, 134 (1995)].

describing the bonding in a noble gas solid would be to simply sum up the pairwise bonding contributions between all atoms in the solid. Since all atoms are equivalent, this corresponds to summing up the contributions from all other atoms as experienced by an arbitrary atom, which we take to be located at $\mathbf{R} = 0$. For the energy per atom we then obtain

$$\frac{E}{M} \simeq \frac{1}{2} \sum_{\mathbf{R} \neq 0} E_2^{\mathrm{LJ}}(|\mathbf{R}|) \quad , \tag{6.5}$$

where the factor 1/2 corrects for double-counting. We immediately stress that considering only the (purely distance dependent) pair interaction is a gross simplification. In general, any additional particle will affect the electron density of all atoms in its neighborhood, and thereby also modify the pairwise interactions among the latter. This is exactly, why one needs in principle a new self-consistent calculation for each atomic configuration. Expanding the total energy in terms of interactions between all particles, it can, however, be taken into account by including so-called three-body or even higher order many-body interactions. We will find such terms necessary in the other bonding classes, but for the noble gases the restriction to pairwise interaction should be quite o.k. (which will be verified below). This has to do with that the van der Waals interaction is quite weak. As long as the particles do not approach each other too closely, the wavefunctions remain quite undisturbed from the form in the free atom. Adding more particles in the vicinity of other particles does therefore not affect the electron densities of the latter significantly (they are in fact still quite similar to their atomic forms anyway), and correspondingly a pairwise sum is expected to describe the total energy quite well.
If we insert the exact form of the Lennard-Jones potential from eq. (6.4), we obtain for

	sc	bcc	fcc
NN	6	8	12
A_6	8.40	12.25	14.45
A_{12}	6.20	9.11	12.13
$A_6^2/2A_{12}$	5.69	8.24	8.61

Table 6.1: Number of nearest neighbors, NN, and lattice sums for the three cubic Bravais lattices. The final row is proportional to the energy of the crystal. Further lattice sum values for other n can be found in Ashcroft/Mermin.

the energy per atom in the pair potential approximation

$$\frac{E}{M} \;=\; 2\varepsilon \sum_{I=2}^{M} \left\{ \left(\frac{\sigma}{|\mathbf{R}_I|} \right)^{12} \;-\; \left(\frac{\sigma}{|\mathbf{R}_I|} \right)^{6} \right\} \quad . \tag{6.6}$$

It is useful to rewrite this expression in a form, which allows to evaluate the sum over all atoms in a general form for a given crystal structure. We therefore introduce the dimensionless quantity α_I,

$$|\mathbf{R}_I| \;=\; \alpha_I \cdot c, \tag{6.7}$$

where c is the distance to the nearest neighbor in the considered crystal structure. With this, the energy per atom can be written

$$\frac{E(c)^{\mathrm{crystal}}}{M} \;=\; 2\varepsilon \left\{ \left(\frac{\sigma}{c} \right)^{12} A_{12}^{\mathrm{crystal}} \;-\; \left(\frac{\sigma}{c} \right)^{6} A_{6}^{\mathrm{crystal}} \right\} \quad . \tag{6.8}$$

The energy is then just a function of the nearest neighbor distance, and all the information about the particular crystal structure (i.e. number of neighbors in nearest, next-nearest etc. shells) is contained in the lattice sum

$$A_n^{\mathrm{crystal}} \;=\; \sum_{I \in \mathrm{crystal}} \alpha_I^{-n}. \tag{6.9}$$

As an illustration let us evaluate this lattice sum for the fcc crystal structure. In this lattice type we have 12 nearest neighbors at distance c ($= a_{\mathrm{fcc}}/\sqrt{2}$, where a_{fcc} is the lattice constant). Then we have 6 next-nearest neighbors at a distance $\sqrt{2}c$, and so forth. Hence, the α_I for the first two shells are 1 and $\sqrt{2}$, cf. eq. (6.7). Obviously, for more distant neighbor shells, the α_I successively become larger, and correspondingly their contribution to the lattice sum smaller (inverse power!). For A_{12}^{fcc} we arrive therefore at

$$A_{12}^{\mathrm{fcc}} \;=\; 12 \cdot (1)^{-12} \;+\; 6 \cdot (\sqrt{2})^{-12} \;+\; \ldots \;=\; 12.13 \quad . \tag{6.10}$$

The lattice sum is thus already quite well approximated by only the first nearest neighbor shell. This is a consequence of the high power $n = 12$ considered in A_{12}. In fact, $A_{\mathrm{n}\to\infty}$ is exactly given by the number of nearest neighbors. For lower n, on the other hand, the more distant neighbor shells contribute more significantly, as can be seen from Table 6.1.

	Ne	Ar	Kr	Xe
c_o (theory)	3.13 Å	3.75 Å	3.99 Å	4.33 Å
c_o (exp.)	2.99 Å	3.71 Å	3.98 Å	4.34 Å
$E^{\rm coh}$ (theory)	27 meV	89 meV	120 mev	172 meV
$E^{\rm coh}$ (exp.)	20 meV	80 meV	110 mev	170 meV

Table 6.2: Equilibrium nearest neighbor distance c_o and cohesive energy $E^{\rm coh}$ of the noble gases, as resulting from experiment and the pair potential approximation discussed in the text (theory). The larger deviation of c_o for the lightest element Ne is due to zero-point vibrations, which are neglected in the theory [from Ashcroft and Mermin].

From the general form of eq. (6.8) it is straightforward to deduce the equilibrium nearest neighbor spacing c_o and the cohesive energy for any given crystal structure,

$$\begin{aligned} \left.\frac{dE^{\rm crystal}(c)}{dc}\right|_{c_o} &= 0 \quad \Rightarrow \quad c_o = \sigma \left(\frac{2A_{12}^{\rm crystal}}{A_6^{\rm crystal}}\right)^{1/6} \\ E^{\rm coh,crystal} &= -\frac{E^{\rm crystal}(c_o)}{M} = \varepsilon \frac{(A_6^{\rm crystal})^2}{2A_{12}}. \end{aligned} \tag{6.11}$$

The cohesive energy for a particular element (entering only via ε!) in a given crystal lattice is therefore only dependent on the fraction of lattice sums, $\frac{(A_6^{\rm crystal})^2}{2A_{12}}$. The lattice maximizing this fraction will correspondingly be the most stable one. Inspecting Table 6.1 we find that this is the case for the fcc structure. We have to note, however, that the hcp lattice has highly similar lattice sums (deviating only in the third digits). The crudeness of the approach does not allow to distinguish between such subtle differences. All we can conclude therefore, is that van der Waals bonding will favor closed packed lattice structures, which is ultimately a consequence of the underlying non-directional pair interaction.

All noble gases (except for He) solidify indeed into an fcc structure. Using the parameters σ and ε obtained by fitting the Lennard-Jones curve to low-density gas phase data or the quantum chemistry calculations of the diatomic molecules, we obtain the cohesive energies and lattice constants listed in Table 6.2. Considering the simplicity of our pair potential model, the agreement is quite good (roughly at the 10% level). At the obtained quite large equilibrium bond lengths, the wave function overlap is indeed minimal (as anticipated). The energy levels in a noble gas solid will therefore show only a small broadening compared to the atomic limit as explained in Fig. 6.6. Due to the large energy difference between the uppermost occupied and the lowermost unoccupied band, noble gas crystals will behave as an insulator. On the basis of a crude pair potential we can thus understand quite some fundamental cohesive (and even electronic) properties of the noble metals solids. This is gratifying in this special case, but we will see that it is more an exception, than a rule.

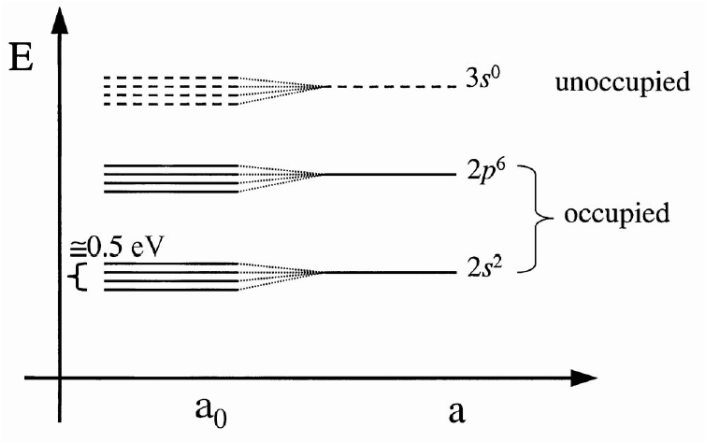

Figure 6.6: Sketch of the energy levels of a noble gas crystal, using the example of Neon. In the atomic limit a, all shells are filled. Even at the equilibrium lattice constant a_o the interaction between the atoms is weak, and the electronic states are only broadened by a small amount. This still leaves a large energy gap between occupied and unoccupied states, and Neon results as an insulator.

6.3 Ionic bonding

Atoms and ions with closed shells are particularly stable, i.e. a lot of energy is required to excite an electron from a filled shell into an unoccupied state. The conceptual idea behind ionic bonding is therefore that electrons are exchanged in such a way, that the involved atoms reach this stable closed shell state. This is most easily realized for the so-called ionic crystals formed of alkali halides (i.e. Group I and VII elements of the periodic system). Take NaCl as an example. The model conception is then, that Na with the electron configuration of $[1s^2 2s^2 2p^6]3s^1$ becomes a Na^+ ion, and Cl $[1s^2 2s^2 2p^6]3s^2 3p^5$ a Cl^- ion, thereby achieving the closed shell configuration in both cases. Similar ideas would, e.g., also hold for II-VI compounds. With this electron transfer accomplished, we arrive at a situation that is quite similar to the one discussed in the last section: the interaction between two filled shell particles. As soon as they come too close together (something that is now more determined by the ionic radii and not the atomic radii, though), hard core repulsion will set in. Contrary to the van der Waals case, the attractive interaction is, however, not anymore due to just the weak dipole fluctuations, but instead primarily due to the much stronger electrostatic attraction between the differently charged ions. If this electrostatic attraction is stronger than the cost of exchanging the electrons between the atoms to reach the ionic states in the first place, then the crystal will hold together. Ionic bonding is therefore most effective, if the cost to create the ions is low, i.e. when one atom type readily gives away electrons (low ionization potential) and the other one readily takes them (high electron affinity).

In this most naive perception an ionic crystal is in other words simply a collection of impenetrable charged spheres, glued together by electrostatic interaction. In analogy to the van der Waals case, we thus expect the interaction between two ions of opposite charge to arise out of a repulsive and an attractive part. The repulsive part is due to Pauli

Structure	$A_{\rm Mad}$	NN
Cesium chloride	1.76	8
Sodium chloride	1.75	6
Wurtzite	1.64	4
Zincblende	1.64	4

Table 6.3: Madelung constants $A_{\rm Mad}$ and nearest-neighbor coordination NN for the most common ionic crystal structures.

repulsion, and since electrostatic interaction is much stronger than the (also existing) van der Waals forces, the attractive part will be predominantly given by a Coulomb $1/r$-potential

$$E_2^{\rm ionic}(r) \;=\; E^{\rm rep.} + E^{\rm attr.} \;=\; \frac{C}{r^{12}} - \frac{e^2}{4\pi\epsilon_o\, r} \quad , \tag{6.12}$$

where we have simply taken the charge on the ions as $\pm e$, and $\epsilon_o = 8.85 \cdot 10^{-12}\,{\rm As/Vm}$ is the dielectric constant of vacuum. Note, that evaluating the constants in the attractive term leads to $E^{\rm attr.} = -14.4\,{\rm eV}/[r \text{ in Å}]$, i.e. bringing the two ions together at a distance of 3 Å yields already about 5 eV electrostatic energy gain. The cost to create Na^+ and Cl^- (difference of electron affinity and ionization potential) is only $\sim 1.5\,{\rm eV}$, leaving still quite a lot of energy gain to form a very stable bond. Just like in the van der Waals case, one has to recognize of course that the $1/r^{12}$ repulsive potential is only a rough convenient choice. One can determine the proportionality constant C by fitting either to first-principles calculations or to compressibility data. One then often finds, that using smaller inverse powers somewhere in the range 6-10 or an exponential form (Born-Meyer potential) can fit the data even better. For the general discussion on the chemical bonding intended here, such multiparameter fits are, however, not very illuminating, and we will stick for simplicity to the $1/r^{12}$-potential already used in the van der Waals case.
Having obtained the interaction between an ion pair, we may employ the same reasoning as in the last section to determine the cohesive energy of an ionic solid. Again, we do not expect dramatic charge rearrangements in the solid compared to the case of the isolated (closed-shell) ions. A simple sum over the pairwise contributions as in eq. (6.5) should therefore already describe the energy per ion pair quite well. This leads to

$$\frac{E}{M} \;\simeq\; \frac{1}{2}\sum_{\mathbf{R}\neq 0} E_2^{\rm ionic}(|\mathbf{R}|) \;=\; \sum_{I=2}^{M}\left\{\frac{C}{r^{12}} - \frac{\pm 1}{4\pi\epsilon_o\, r}\right\} \quad , \tag{6.13}$$

where the ± 1 applies when the ion I in the sum has negative or positive charge, respectively. As before, we proceed by eliminating the properties exclusively due to the crystal structure through the definition of the dimensionless quantity α_I (cf. eq. (6.7)) and arrive at

$$\frac{E(c)^{\rm crystal}}{M} \;=\; \left\{\frac{C}{c^{12}} A_{12}^{\rm crystal} \;-\; \frac{e^2}{4\pi\epsilon_o\, c} A_{\rm Mad}^{\rm crystal}\right\} \quad . \tag{6.14}$$

Similar to the lattice sums $A_n^{\rm crystal}$ defined in eq. (6.9), the complete information about the neighbor shells of ions with positive or negative charges in the particular crystal structure

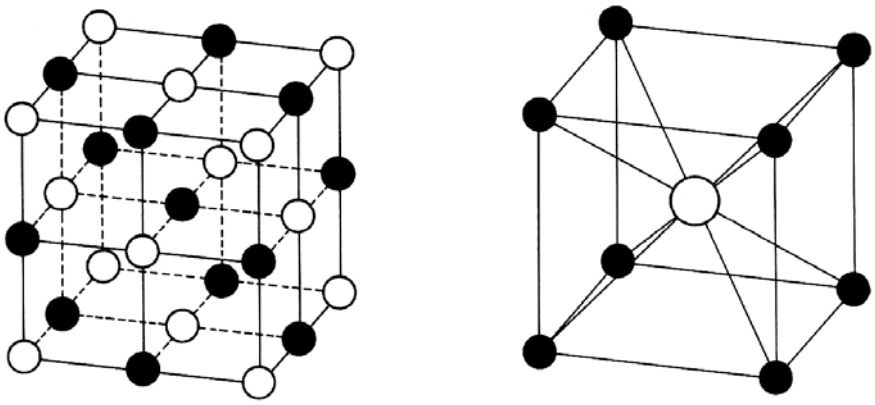

Figure 6.7: Two most common ionic crystal lattices: Sodium chloride (left) and Cesium chloride (right).

are now summarized in the so-called *Madelung constant*

$$A_{\mathrm{Mad}}^{\mathrm{crystal}} = \sum_{I \in \mathrm{crystal}} \frac{\pm 1}{\alpha_I}. \tag{6.15}$$

Apparently, this Madelung constant is the equivalent of the lattice sum A_1^{crystal}, taking additionally into account that neighboring ions with positive or negative charge contribute differently to the electrostatic interaction in the lattice. Unfortunately, the weak decrease (or long range) of the $1/r$ potential makes the actual calculation of Madelung constants much more tricky compared to the one of lattice sums. Depending on the way the summation is carried out, any value whatsoever can be obtained (corresponding to finite crystals with differing surface charges). The method of choice to avoid such problems is the *Ewald summation* technique already discussed in section 1.3. With this, the Madelung constants of any crystal lattice can readily be computed and Table 6.3 lists a few A_{Mad} for lattice types that will become relevant in the discussion below.
From the structure of eq. (6.14) it is obvious that again the maximum cohesive energy will be obtained by close-packed structures, which maximize both the lattice sum A_{12} and the Madelung constant. As already noted in the last section, this follows simply from the still non-directional bonding implied by the interionic pair potential $E_2^{\mathrm{ionic}}(r)$. Since the nearest neighbor shell contributes most strongly to A_{12} *and* A_{Mad}, but only ions of opposite charge yield electrostatic attraction, ionic crystals will more specifically prefer those close-packed structures in which each ion is surrounded by a shell of ions with opposite charge. Fig. 6.7 shows the two crystal structures that fulfill these close-packing and opposite ion shell requirements to an optimum. The sodium chloride (rocksalt) structure consists of two interpenetrating fcc lattices, thus achieving a coordination of 6 per ion, while the cesium chloride structure can be viewed as a bcc lattice with the ion of second type inhabitating the interior of the cube (coordination 8).
Table 6.3 lists the Madelung constants and coordination numbers of these two, and two less dense lattices (zincblende and wurtzite). As already discussed in the context of the lattice sum A_1, the Madelung constant is expected to scale with the coordination number, but not as clearly as for example A_{12}. The contribution of second and further

Compound	c_o(exp)	E^{Mad}	E^{coh}(theory)	E^{coh}(exp)
LiF	2.01 Å	-11.81 eV	10.83 eV	11.45 eV
LiCl	2.57 Å	-9.65 eV	8.85 eV	8.98 eV
LiBr	2.75 Å	-9.28 eV	8.51 eV	8.39 eV
LiI	3.01 Å	-8.64 eV	7.92 eV	7.66 eV
NaF	2.32 Å	-10.49 eV	9.62 eV	9.96 eV
NaCl	2.82 Å	-8.32 eV	8.18 eV	8.18 eV
NaBr	2.99 Å	-8.52 eV	7.81 eV	7.72 eV
NaI	3.24 Å	-7.39 eV	7.32 eV	7.13 eV

Table 6.4: Experimental lattice constants c_o, Madelung electrostatic energies E^{Mad}, theoretical cohesive energies per ion pair E^{coh}(theory), cf. eq. (6.16), and experimental cohesive energies per ion pair E^{coh}(exp) for a number of alkali halides crystallizing in the sodium chloride lattice. The larger the ionic radii, the larger the lattice constant, and accordingly the lower the cohesive energy becomes. The largest part to the cohesive energy comes indeed from the electrostatic Madelung energy.

neighbors is still significant, leading to highly similar Madelung constants for the 8fold and 6fold coordinated CsCl and NaCl lattices (only the 4fold coordinated zincblende and wurtzite structures exhibit a noticeably lower A_{Mad}). The rough pair potential theory does therefore not allow to distinguish between the two dense lattices, in which indeed the large majority of alkali halides and II-VI elements solidify. Most of the exceptions that crystallize for example in the wurtzite or zincblende lattice can nevertheless still be understood on the basis of our simple analysis, taking the additional constraint of largely different ionic radii of the two atom/ion species into account: The hard-core repulsion does in those cases not allow the denser packing, which becomes intuitively clear when simply drawing a closed-packed structure with circles of very different sizes in two dimensions. Leaving aside this influence on the specific crystalline arrangement chosen, the dominant contribution to the cohesive energy comes in any case from the electrostatic interaction (also often called Madelung energy E^{Mad}). This can be discerned by evaluating it at the experimentally determined lattice constant c_o. Using a strategy as in eqs. (6.11), one finds furthermore that the total cohesive energy at this experimental lattice constant is

$$E^{\mathrm{coh,crystal}} = -\frac{E^{\mathrm{crystal}}(c_o)}{M} = -\frac{11}{12}E^{\mathrm{Mad}}(c_o) = \frac{11}{12}\frac{A_{\mathrm{Mad}}e^2}{4\pi\epsilon_o c_o} \quad . \tag{6.16}$$

Table 6.4 lists this energy and the Madelung energy for a number of alkali halides, and compares with experiment. The agreement is not as good as the one obtained in the previous section for the molecular crystals, but given the simplicity of the theoretical model, it is obvious that the essential physics are still contained in it. The remaining 10-20% of the binding comes from overlapping and hybridized wave functions, which is for example reflected in the noticeable broadening of the energy levels as shown for KCl in Fig. 6.8. Still, the broadening is still much smaller than the separation between the individual levels, and consequently the alkali halides are insulators. Again, the only small overlap of the ionic charge distributions and correspondingly small charge rearrangements compared to the isolated ions, is the reason why the primitive pair potential approach

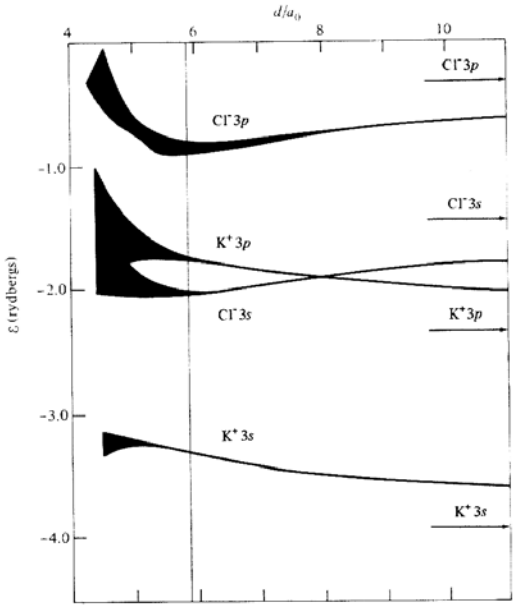

Figure 6.8: Calculated energy levels of a KCl-crystal as a function of the interionic distance d (measured in Bohr radii, a_o). The vertical line is the experimental value, and the ionic levels are indicated by arrows on the right-hand side. The valence band derives from the full Cl $3p$ shell, and at the experimental lattice constant a noticeable, but still small level broadening is discernible [from L.P. Howard, Phys. Rev. **109**, 1927 (1958)].

works so well for these systems. Further discussions on these aspects can be found in J.A. Majewski and P. Vogl, Phys. Rev. Lett. **57**, 1366 (1986); Phys. Rev. B **35**, 9666 (1987).

6.4 Covalent bonding

The ionic bonding described in the last section is based on a complete electron transfer between the atoms involved in the bond. An electron is thus shared, but not at all evenly. The somewhat opposite case (still in our idealized pictures), i.e. when chemical binding arises out of electrons being equally shared between the bonding partners, is called *covalence*. Contrary to the ionic case, where the electron density in the solid does not differ appreciably from the one of the once formed isolated ions, covalent bonding results from a strong overlap of the atomic-like wavefunctions of the different atoms. The valence electron density is therefore increased *between* the atoms, in contrast to the hitherto discussed van der Waals and ionic bonding types. It is intuitive that such an overlap will also depend on the orbital character of the wavefunctions involved, i.e. in which directions the bonding partners lie. Intrinsic to covalent bonding is therefore a strong *directionality* as opposed to the non-directional ionic or van der Waals bonds. From this understanding, we can immediately draw some conclusions:

- When directionality matters, the preferred crystal structures will not simply result from an optimum packing fraction (leading to fcc, hcp or CsCl, NaCl lattices). The classic examples of covalent bonding, the group IV elements (C, Si, Ge) or III-V

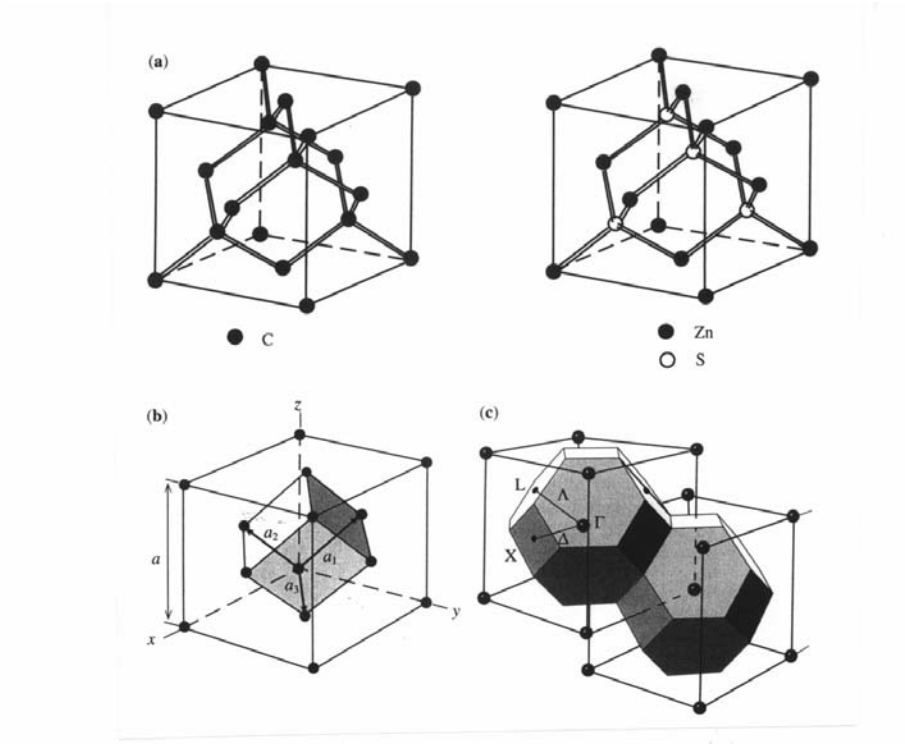

Figure 6.9: Unit-cell of the diamond (upper left) and zincblende (upper right) lattice. They differ only in the atomic species present at the lattice sites (diamond = one species, zincblende = two different species). Each atom has four nearest neighbors and the point group symmetry is T_d. Both lattices derive from an fcc structure with a two atom basis (at (0,0,0) and (1/4, 1/4, 1/4)), as illustrated in the bottom left panel. The lower right figure shows the corresponding Brillouin zone, and some high symmetry points and lines.

compounds (GaAs, GaP), solidify indeed in more open structures like diamond or zincblende, cf. Fig. 6.9.

- Due to the strong directional bonds, the displacement of atoms against each other (shear etc.) will on average be more difficult (at least more difficult than in the case of metals discussed below). Covalent crystals are therefore quite brittle.

- Directionality can not be described by only distance-dependent pair potentials. A theory of cohesion in covalent crystals will therefore be significantly more complicated than the crude pair potential approach that we found so successful to describe van der Waals and ionic crystals. In the language of interatomic potentials, there will be no way around introducing at least threebody, if not higher many-body terms. In fact, the common theme of interatomic potentials for covalent crystals, like the famous Stillinger-Weber potentials or the ubiquitous force-fields, are three-body terms that take angular components into account. Even then, the success and value of using such potentials is completely different compared to the pair potentials of the last two sections: For the latter we found that one general form can treat quite a range of situations and elements very well. Even for the best covalent inter-

Element		a_o (Å)	$E^{\rm coh}$ (eV/atom)	B_o (Mbar)
C	theory	3,602	7,58	4,33
	exp.	3,567	7,37	4,43
	%diff.	**<1%**	**3%**	**−2%**
Si	theory	5,451	4,67	0,98
	exp.	5,429	4,63	0,99
	%diff.	**<1%**	**1%**	**−1%**
Ge	theory	5,655	4,02	0,73
	exp.	5,652	3,85	0,77
	%diff.	**0,2%**	**4%**	**−5%**

Table 6.5: Comparison DFT/experimental results for structural and cohesive properties of group IV semiconductors in the diamond structure. a_o lattice constant, $E^{\rm coh}$ cohesive energy, and B_o the bulk modulus [from M.T. Yin and M.L. Cohen, Phys. Rev. B **24**, 6121 (1981)].

atomic potentials currently on the market, this *transferability* is much more limited. Although there are parametrizations that can describe one bonding situation for one element extremely well (say Si bulk), they completely fail for another element or for the same element in a different bonding environment (say Si surface). This reflects the fact, that the functional forms employed cannot embrace the changing character of the hybridizing wave functions, or in other words that one needs to explicitly treat the electronic degrees of freedom to really gain understanding. Interatomic potentials are nevertheless frequently (often unfortunately uncritically) employed in materials science research, and quite some effort is dedicated to developing further, improved functional forms that might exhibit a higher transferability and reliability. For our general discussion on bonding and cohesion, such refined potential approaches are, however, not very helpful.

Lacking a model of cohesive energy of comparable simplicity to those of van der Waals or ionic bonding, we have to stick to the more elaborate electronic structure theory descriptions as obtained e.g. with DFT. Fortunately, the latter does at least a remarkably good job in describing covalent crystals, as exemplified for the group IV semiconductors in Table 6.5. Recalling that there is no free parameter in the theory, the agreement is indeed quite impressive and shows that the current exchange-correlation functionals capture most of the essential physics underlying covalent bonding.

This requirement for quantitative calculations does, however, not necessarily prevent us from still attempting to gain some further conceptual understanding of the cohesive properties of covalent crystals. We only have to analyze the electronic structure data provided by a DFT calculation in more detail. Let us exemplify how this is done first for the ubiquitous semiconductor material Si. In the beginning of this chapter, we had already discussed how the stable crystal structure and the cohesive energy can be obtained from computed total energy curves in many different crystal lattices, cf. Fig. 6.1. Fig. 6.10 shows the corresponding data for Si. Apparently, the diamond lattice is correctly found to be most stable, and the good agreement of the lattice constant, cohesive energy and bulk modulus with the experimental values were already mentioned in connection with

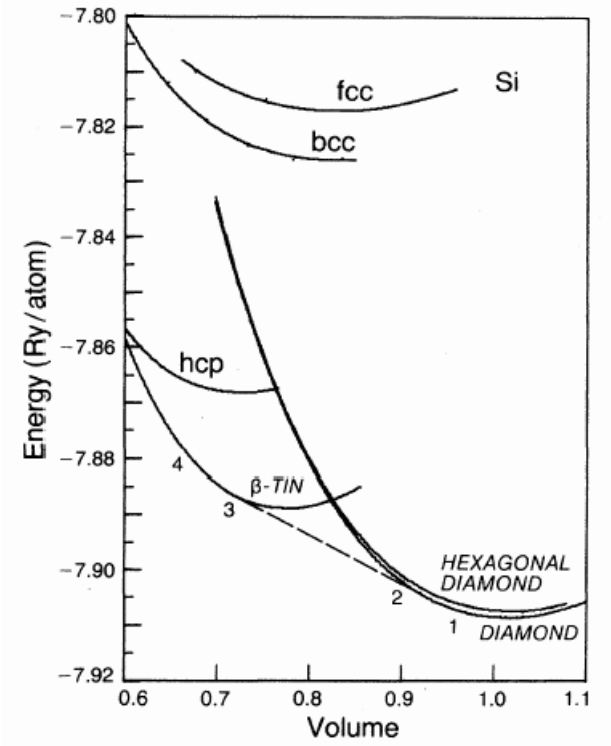

Figure 6.10: DFT-LDA total energy versus volume for Si in various crystal lattices. The volume is normalized to the experimental volume of Si in the diamond lattice. The dashed line explains the common-tangent construction for the phase transition to the $\beta - tin$ structure at elevated pressures [from M.T. Yin and M.L. Cohen, Phys. Rev. Lett. **45**, 1004 (1980)].

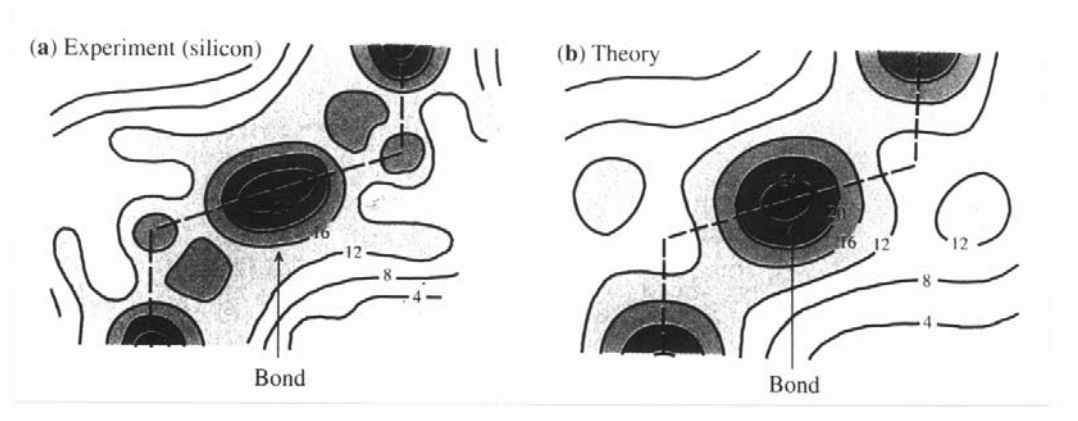

Figure 6.11: Valence electron density (in e per unit-cell volume) for Si from experiment (X-ray diffraction) and theory (DFT-LDA). The characteristic covalent charge increase between the atoms is easily discerned.

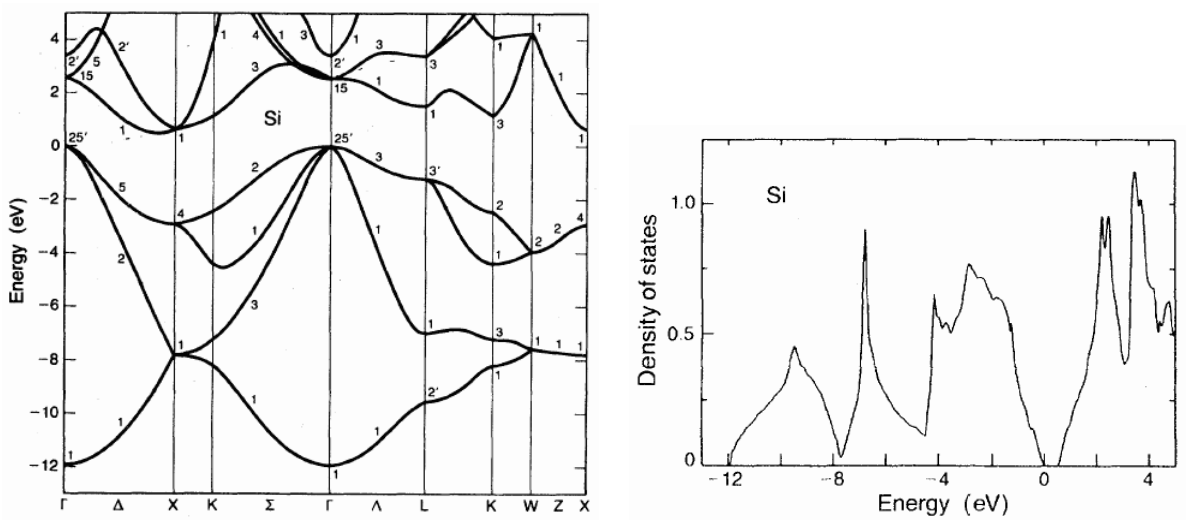

Figure 6.12: DFT-LDA band structure (left) and density of states (right) for Si in the diamond structure. The energy zero corresponds to the top of the valence band. Valence states below -8 eV have s character, and above -4 eV p character. The range in between exhibits strong sp mixing [from M.T. Yin and M.L. Cohen, Phys. Rev. B **26**, 5668 (1982)].

Table 6.5. The computed and measured valence electron density in the stable diamond structure is displayed in Fig. 6.11, from which the expected charge increase between the atoms, characteristic for covalent bonding, can be discerned. This indicates a strong hybridization of the valence atomic orbitals, which is also reflected in the calculated band structure and density of states, shown in Fig. 6.12. The pronounced mixing of $s-p$ states (and the larger p than s character of the valence band) tells that it makes no sense anymore to discuss the Si valence electronic structure in terms of its atomic ground state electronic configuration [Ne] $3s^2 3p^2$. What is often found instead for covalent crystals, is that it is more instructive to use so-called *hybrid orbitals* as a basis for the discussion. These correspond to the orbitals of an excited state of the atom, and in the case of Si in the diamond structure, this excited state would be the one, where one valence s electron is pushed into the valence p level. The resulting so-called sp^3*-hybrid functions* are

$$\sigma_1 = \frac{1}{2}(s + p_x + p_y + p_z) \tag{6.17}$$

$$\sigma_2 = \frac{1}{2}(s + p_x - p_y - p_z) \tag{6.18}$$

$$\sigma_3 = \frac{1}{2}(s - p_x + p_y - p_z) \tag{6.19}$$

$$\sigma_4 = \frac{1}{2}(s - p_x - p_y + p_z) \tag{6.20}$$

They point in the four directions of a tetrahedron as schematized in Fig. 6.13, and are more directional and of longer range compared to the ground state s and p atomic orbitals. Correspondingly, they are perfectly suited for the diamond structure, and the higher energy gain through the chemical bonding outweighs apparently the energy that

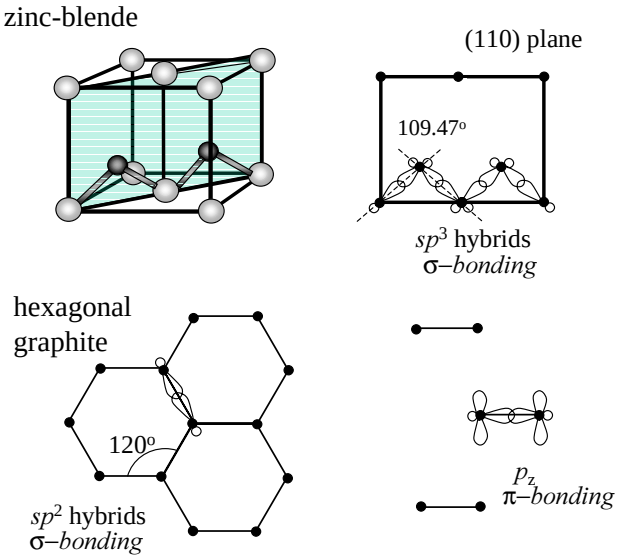

Figure 6.13: Illustration of the tetrahedral sp^3 bonding arrangement in the zincblende/diamond structure (upper), and the sp^2p_z bonding in the layered graphite structure (lower). For graphite, a top (in the plane of the layers) and a side view (perpendicular to the layers) is shown.

is required initially to promote the s electrons to the p levels.

Whereas this picture of sp^3-hybrids renders the high stability of the diamond structure and its high p valence character comprehensible, there is unfortunately no simple rule that would predict, which hybrid orbital set (and corresponding structure) is most preferred for which element. Hybrid functionals are thus no real explanation for cohesive properties, but "just" a suitable language for describing the bonding properties. Another possible hybrid orbital set for group IV (s^2p^2) elements is for example the sp^2p_z set, cf. Fig. 6.13, which is used to discuss layered structures like graphite. Similar to this, we have also to admit that there is (yet?) no simple theory concerning the conductive properties of covalent crystals. The moderate band gap between the topmost occupied fourth band ($\Gamma_{25'}$) and the lowest unoccupied fifth band (X_1) in the Si band structure in Fig. 6.12 explains its semiconducting nature (recall that there are two atoms per diamond unit cell, and correspondingly eight valence electrons). Whether such a gap opens or whether for example the point L, Γ or X exhibits the lowest conduction band state depends on the other hand intricately on the material (Ge, GaAs, Si), and can only be obtained by quantitative electronic structure calculations like DFT.

Having said that, let us continue with what we can understand and learn about covalent crystals. Up to now we had always simply called the lowest energy crystal structure "the stable one". In principle one has to be more specific here, as the crystal structure can obviously depend on the environmental condition, i.e. temperature T and pressure p. With respect to temperature we had already said, that we restrict ourselves in this chapter to sufficiently low temperatures to render vibrational contributions insignificant. We have not, however, mentioned a possible pressure dependence yet. Our previous argument was

always based exclusively on the total energy; hence, our conclusions would correspond to the limit of zero (or low) pressure. At finite (higher) pressures, we do not expect drastic changes for the close-packed van der Waals and ionic crystals either. They are already close-packed, and pushing the atoms even more closely together as a consequence of external pressure would only make them run into the hard core repulsion, thus preventing qualitative structural changes. The situation for the now discussed covalent crystals is quite different, though. Here, we find more open lattice types as a consequence of the directional bonding and might wonder, whether external pressure might not be able to squeeze them together quite a bit, or even induce *structural phase transitions* into denser lattices. Hence, we have to address the influence of pressure a bit more in detail.
The generalization to finite pressure and temperature leads us automatically to thermodynamics. Instead of just the total energy argument, the latter tells us that the ground state (in the constant (T,p)-ensemble) is characterized as minimizing the Gibb's free energy

$$G(T,p) \;=\; U \;-\; TS \;+\; pV \;=\; E \;+\; E^{\mathrm{vib}}(T) \;-\; TS \;+\; pV \quad . \tag{6.21}$$

Here, U is the internal energy, which receives contributions from the total (electronic) energy E and from the energy of lattice vibrations $E^{\mathrm{vib}}(T)$. S is the entropy, to which again the vibrations contribute (but for example also the configurational entropy due to defects). In our restriction to low temperatures we dont have to worry much about the temperature dependent contributions. This is in fact not exactly correct, because the zero-point energy of the vibrations will always contribute. We will neglect it here, nevertheless. Then we are left with the fact that the most stable structure will minimize

$$G(T \to 0,p) \;\approx\; E \;+\; pV \;=\; H \quad , \tag{6.22}$$

i.e. the enthalpy H.
In this form we clearly see, how a high external pressure can induce a structural phase transition: Even though an open structure might minimize the total energy E, its large volume V still increases the enthalpy quite a bit at high pressures. Another more dense structure with a higher energy, but a smaller volume can then possibly still yield in total a lower enthalpy. How can we now quantify, if and when this will be the case? First we recognize that from the well-known formula of adiabatic work ($0 = dQ = dE - TdS + pdV$) follows that

$$\frac{\partial E}{\partial V} \;=\; -p. \tag{6.23}$$

If we thus plot the total energy as a function of volume, as done e.g. in Fig. 6.10, the slope at any V will give us the pressure to which this volume corresponds. In other words, any applied external pressure p will bring us to the point in the total energy curve, the slope of which is equal to p. Obviously, this way we can climb up only on the left branch of the curve: External pressure larger than zero will only decrease the volume. Correspondingly, any slope on the right branch would yield a negative pressure, which is unphysical. It is also intuitive to see, that in a wide and shallow minimum a given pressure will yield a much larger volume compression compared to a narrow and steep minimum (the same slope value corresponding to p needs to be reached!).
With this understanding, we can already predict the equilibrium volume at any finite pressure p for a given lattice type. Yet, what happens if we compare different lattice types? At the point of transition from one crystal structure to the other, both will exhibit the

same H at the same p. The same p implies, however, that both lattices exhibit the same slope $\partial E/\partial V$. This is exploited in the famous *common tangent (or Maxwell, or Gibb's) construction* for a graphical solution of this problem. Consider the situation illustrated in Fig. 6.10 for the diamond and β-tin curves. A common tangent is drawn between the total energy curve of the lowest energy lattice (diamond) and the curve of another higher energy lattice (β-tin). This means that the volumes $V_{\rm diam}$ and $V_{\beta-{\rm tin}}$ at the crossing points of the tangent with the two curves correspond to the equilibrium volumes of the two lattices at the same pressure p. Furthermore, the difference in total energy at these two points $E_{\rm diam}(V_{\rm diam}) - E_{\beta-{\rm tin}}(V_{\beta-{\rm tin}})$ is just given by $-p(V_{\rm diam} - V_{\beta-{\rm tin}})$ (slope times volume difference!). Yet, this means

$$E_{\rm diam}(V_{\rm diam}) - E_{\beta-{\rm tin}}(V_{\beta-{\rm tin}}) \;=\; -\,p(V_{\rm diam} - V_{\beta-{\rm tin}}) \quad , \tag{6.24}$$

which upon rearranging becomes simply $H_{\rm diam} = H_{\beta-{\rm tin}}$, i.e. at this pressure p the two lattices are in equilibrium and we have identified the structural phase transition.
Generalizing we can thus say, that if we can find a common tangent to two total energy versus volume curves, there will be a phase transition from the lattice of lower total energy to the one of higher total energy at the pressure p given by the slope of the tangent. For this, the curves necessarily need to cross at some smaller volume, i.e. if all higher energy lattice curves stay above the lowest energy one for all lower volumes, there will never be a pressure induced phase transition. Inspecting Fig. 6.1 for tungsten, we find this to be the case (as expected). For Si, on the other hand, such a common tangent is found to the β-tin lattice, cf. Fig. 6.10. Evaluating the pressure from the slope one obtains $p_{\rm trans} = 99\,{\rm kbar}$, which is in excellent agreement with experiment, where this transition is indeed observed at 125 kbar. It is also interesting to note, that although the hexagonal diamond (wurtzite) lattice exhibits a energy that is very similar to the diamond lattice, cf. Fig. 6.10, there will never be a phase transition to it, on the other hand, because its curve always lies within the diamond one.
Such insights into high pressure phase transitions are a first example of how a combination of DFT with thermodynamic considerations can transport the predictive power of the first-principles electronic structure technique to finite temperatures and pressures. We will see more examples of such combinations in later chapters of this lecture, but for the moment let us return to the cohesive property discussion. Having learnt a lot for the element Si, one can ask how general this is concerning other covalent crystals. After all, we recall that we could apply more or less the same reasoning for all van der Waals and ionic crystals. Here, we are again disappointed by the significantly increased complexity of covalent bonding, though. While very similar properties are obtained for the lower group IV neighbor Ge, one finds that the computed total energy versus volume curves for the upper neighbor C have quite different positions, cf. Fig. 6.14. In turn, the diamond structure is still very stable, but no phase transition to the β-tin lattice is possible. Similarly, the bulk modulus for C is a factor of four higher than the one of Si and Ge, cf. Table 6.5. All three elements are sp^3-bonded, so why is C so much different than Si and Ge? The reason lies in the different core shell structure. This closed-shell consists only of $1s^2$ in the case of C, i.e. there are no p states in the core. The valence $2p$ states can therefore (without orthogonalization problems) penetrate relatively far into the region of the nucleus and thereby hybridize with the $2s$ orbitals. For Si and Ge, on the other hand, the closed-shell contains p states (Si: $2p$, Ge: $2p$ and $3p$), and therefore the $3p$ (or respectively $4p$) valence electrons are kept away from the region closer to the core. Furthermore, the first

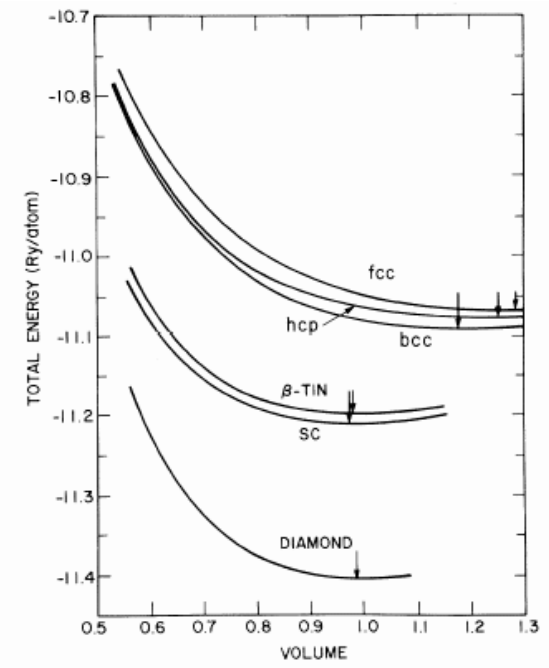

Figure 6.14: DFT-LDA total energy versus volume for C in various crystal lattices. The volume is normalized to the experimental volume of C in the diamond lattice [from M.T. Yin and M.L. Cohen, Phys. Rev. Lett. **50**, 2006 (1983)].

unoccupied states of C are the $3s$ states (the second shell has only s and p states). For Si and Ge, however, there are empty d states in the valence shell. As a consequence, the detailed calculations show, that in Si and Ge the valence wave functions are less directional than in C (due to the lower degree of hybridization), and are not purely sp^3 states, but have some d character admixed. This means that the degree of covalent bonding and the stiffness regarding a change in the bonding angle is much larger for C. Correspondingly, the phase transition to the β-tin phase (with its different bond angles) is suppressed and C is much harder than Si and Ge. We thus see that small variations even in the core electronic structure, the influence of which is commonly depreciated for the bonding, can lead to qualitatively different cohesive properties in covalent crystals. It is obvious that it is hopeless to try to describe this with a pair potential approach.

What we have not yet explicitly considered in the discussion of carbon, is that it is known that the diamond structure is not the true ground state. In fact, the computed DFT-LDA total energy curve for the graphite lattice exhibits indeed a slightly ($\approx 0.02\,\mathrm{eV}$!, M.T. Yin and M.L. Cohen, Phys. Rev. B **29**, 6996 (1984)) lower minimum than the diamond structure (yet, this is NOT the case for Si and Ge). This minimum is, however, at a considerably larger volume ($V_{\mathrm{graphite}} = 1.7\,V_{\mathrm{diam}}$), and therewith even outside of the large volume range shown in Fig. 6.14. This large volume difference explains also the extremely large lifetime of the metastable diamond structure: The way from one structure to the other is only possible via a drastic displacement of all atoms in the lattice and correspondingly connected with a high energy barrier. Going from the open, layered graphite structure to the diamond structure is nevertheless efficiently possible

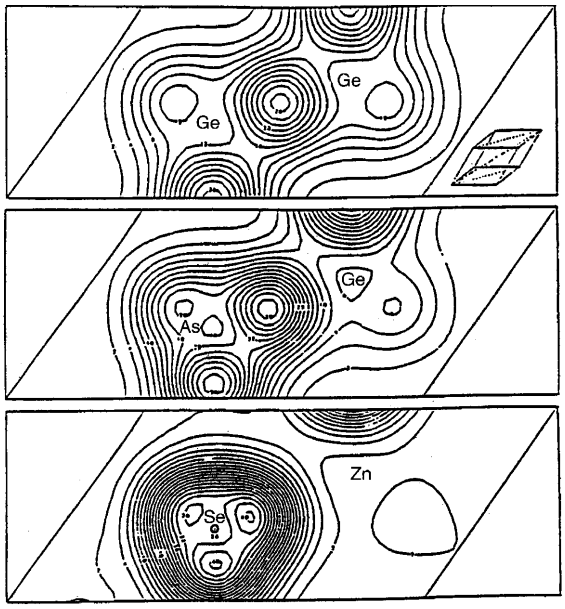

Figure 6.15: Valence electron density of Ge (top), b) GaAs (middle), and c) ZnSe (lower) in e per unit-cell volume.

under very high external pressure (e.g. in the earth core). For the way back, however, only high temperatures can accelerate the transition (through the TS term in the Gibb's free energy), whereas at lower temperatures (representative of our normal living environment), the transition is kinetically inhibited. The large volume connected to the graphite lattice is due to its layered structure. Within one hexagonal layer the interatomic carbon distance is with 1.45 Å even slightly smaller than in the diamond lattice. The distance between the parallel layers is with 3.58 Å much larger, on the other hand, and leads in total to the large atomic volume in graphite. This indicates already that the binding between the layers is quite weak (as expressed in the sp^2p_z hybridization). Along the parallel layers, the crystal should therefore cleave or shift easily. This weak bonding of the p_z orbitals is also the reason for the metallic character of graphite: Due to the strong sp^2 binding within the layer, a strong gap opens up. The p_z states are more delocalized, on the other hand, and give rise to a half-filled band.

Finally, we should stress that the initially mentioned view of ionic and covalent bonding as opposite extremes indicates already, that most real structures will exhibit varying degrees of both bonding types. This is nicely illustrated by the series Ge, GaAs and ZnSe, i.e. a pure group IV, a III-V and a II-V structure all in the same row of the periodic system of elements. Fig. 6.15 shows the corresponding valence electron densities. While the increased bonding density lies in the purely covalent Ge solid still symmetrically between the atoms, the maximum shifts more and more towards the anion for the case of the III-V and II-VI compound. GaAs can still be discussed in the sp^3 picture, e.g. as $Ga^{(-)}(4s^14p^3)$ and $As^{(+)}(4s^14p^3)$. The range of the sp^3 hybrids is, however, larger for the As anion than for the Ga cation, shifting the bonding maximum and giving the bonding a slightly ionic touch. This becomes then even more pronounced for the II-VI compound, and for the I-VII alkali halides discussed in section 6.2, the purely ionic bonding character is attained.

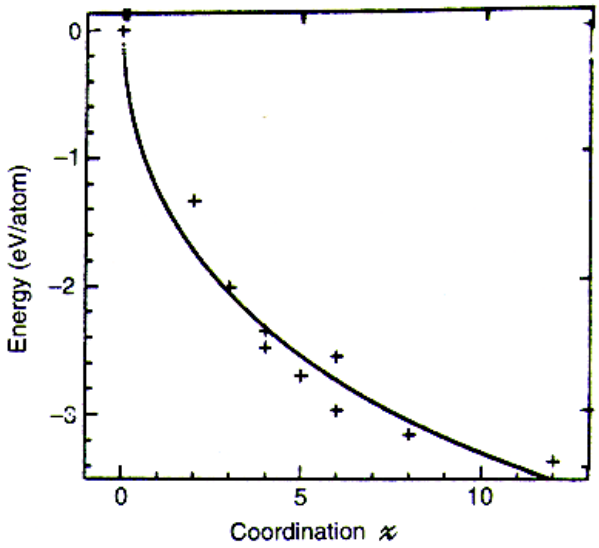

Figure 6.16: DFT-LDA cohesive energy (plotted here as a negative number) for Al as a function of the nearest neighbor coordination NN in various lattice types. The lattice types considered are the linear chain ($NN = 2$), graphite ($NN = 3$), diamond ($NN = 4$), two-dimensional square mesh ($NN = 4$), square bilayer ($NN = 5$), simple cubic ($NN = 6$), triangular mesh ($NN = 6$), vacancy lattice ($NN = 8$) and fcc ($NN = 12$). The solid curve is a fit to $A \cdot (NN) - B\sqrt{NN}$ [from V. Heine *et al.*, Phil. Trans. Royal Soc. (London) **A334**, 393 (1991)].

6.5 Metallic bonding

Although we have already viewed the even or completely one-sided sharing of electrons in covalent and ionic bonding as somewhat opposite extremes, they are similar in the sense that the valence electrons are still quite localized: either on the ions or in the bonds between the atoms. The conceptual idea behind *metallic bonding* is now complementary to this, and describes the situation, when the valence electrons are highly delocalized. In other words they are well shared by a larger number of atoms - in fact one can no longer say to which atom a valence electron really belongs: it is simply part of the "community". Such a situation is for example most closely realized in the alkali metals, which readily give away their only weakly bound s electron in the valence shell. In most abstract terms, such metals can thus be perceived as atomic nuclei immersed in a featureless electron glue. From this understanding, we can immediately (just like in the covalent case) draw a couple of conclusions:

- A delocalized binding is not directional, and should allow for easy displacement of the individual atoms with respect to each other. Metals are therefore rather elastic and ductile.

- Delocalization is the consequence of heavy overlap between the individual valence wave functions. The bands will therefore exhibit a strong dispersion, rendering the opening up of energy gaps in the density of states (DOS) less likely. With the Fermi

Element	a_o (Å)	E^{coh} (eV/atom)	r_s/a_B
Li	3.49	1.63	3.27
Na	4.23	1.11	3.99
K	5.23	0.93	4.95
Rb	5.59	0.85	5.30
Cs	6.05	0.80	5.75

Table 6.6: Experimental values for structural and cohesive properties of group I alkalis in the bcc structure. a_o lattice constant, E^{coh} cohesive energy, and r_s the Wigner-Seitz radius.

level cutting anywhere through this gapless valence DOS, unoccupied states will exist immediately above the highest occupied one. Application of small external perturbations, e.g. an electric field, can then induce current flow, i.e. metals are electric conductors (and in turn also good thermal conductors).

- It is intuitively clear that a contribution arising from delocalized bonding between many atoms can not be described by a sum of pair potentials. This results equally from the understanding that pair potentials are only adequate when there is a negligible distortion of the atomic electron density when the atom is added to the solid. In metals, on the other hand, the overlap between the valence wave functions is so large that the atomic character is hardly recognizable any more. That simple pair potentials will not be appropriate for the description of metallic systems is also nicely visible from plots like the one shown in Fig. 6.16. Here, the cohesive energy for Al is plotted as a function of the nearest neighbor coordination NN in various crystal lattices. If the binding arose only out of pairwise bonds with the nearest neighbors, the cohesive energy would be proportional to NN. What is instead obtained typically as in Fig. 6.16 is that the cohesive energy scales with the coordination more like $A \cdot (NN) - B\sqrt{NN}$, with A and B constant. Apparently, increasing the local coordination about a given atom reduces the strength of the existing bonds, as the delocalized electrons spread more evenly between all neighbors. This phenomenon characteristic for metallic bonding is often called *bond order conservation*, while chemists refer to an *unsaturated* nature of the metallic bond. With pure pair potentials failing, the common theme of interatomic potential schemes used for metals is therefore to add a coordination dependent term, which reduces the linear scaling due to the pair potential for higher coordinated atoms. Most famous examples of such approaches are the so-called Embedded Atom Method (EAM) or Finnis-Sinclair/Bond-Order Potentials (BOPs). Still, the same word of caution holds here as already discussed for the covalent crystals: Although frequently employed in materials sciences, there is yet no really reliable and transferable interatomic potential scheme for metals. Presumably there will never even be one, and real quantitative understanding can only come out of quantum mechanical calculations explicitly treating the electronic degrees of freedom.

As already in the case of covalent bonding, we will have to look for alternatives that will bring us a conceptual understanding of the quantitative data coming out of DFT calcula-

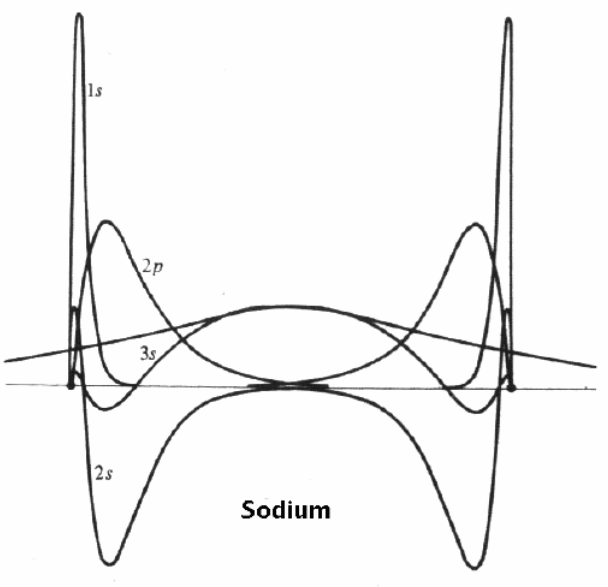

Figure 6.17: Radial wavefunctions of two sodium atoms at the equilibrium interatomic distance they would have in the crystal. There is very small overlap between the $2s$ and $2p$ orbitals, but a very large overlap of the $3s$ valence wave functions [from Ashcroft and Mermin].

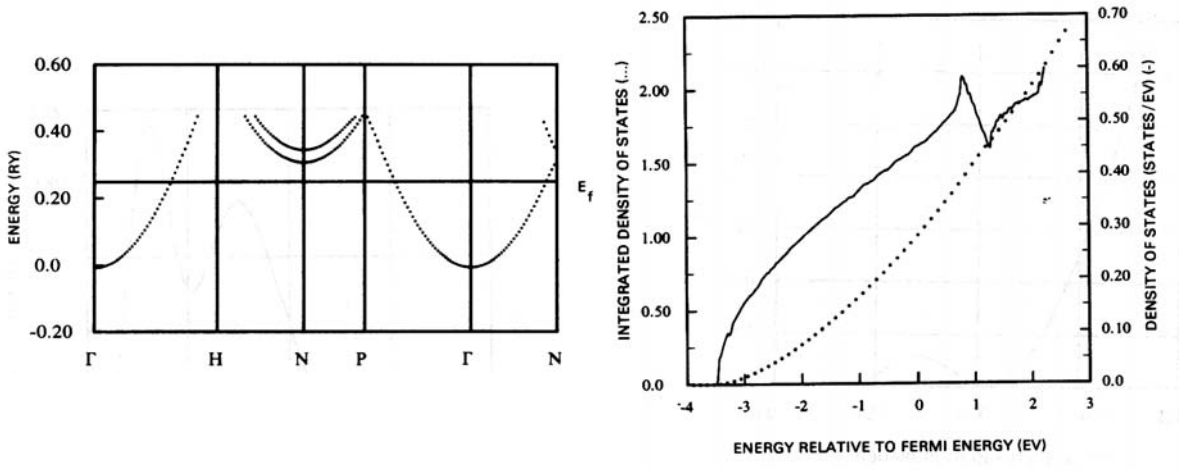

Figure 6.18: DFT-LDA Bandstructure (left) and DOS (right) for Na in the bcc structure. Note how much the valence bands follow a free-electron like dispersion, as also clearly visible in the parabolic shape of the DOS [from V.L. Moruzzi, J.F. Janak and A.R. Williams, *Calculated electronic properties of metals*, Pergamon Press (1978)].

tions. And we will do this first for the so-called *simple* or free-electron like metals, which comprises for example the alkali and earth alkali metals (group I and II). Characteristic data for some alkalis on which we will concentrate is listed in Table 6.6. Fig. 6.17 shows the radial wave functions of two Na atoms at the equilibrium distance they would have in a bcc solid, from which the already mentioned strong overlap of the valence $3s$ states is apparent. In fact, ignoring the oscillations near the two nuclei, the charge distribution of the overlapping $3s$ orbitals can be seen to be practically constant. The band structure of alkalis should therefore exhibit a dispersion very similar to the one of free electrons (hence the name given to these metals), as also illustrated in Fig. 6.18 for Na. It also suggests that the simple jellium model discussed already in chapter 3 could serve as a suitable minimum model to qualitatively describe the bonding in the alkali crystals. In this jellium model, the electron density is considered to be constant over the whole solid, and in its simplest form the ion lattice is equally smeared out to a constant density exactly compensating the electronic charge. The model is then completely specified by just the electron density $n = N/V$, which is usually given in form of the so-called *Wigner-Seitz radius*

$$r_s \;=\; \left(\frac{3}{4\pi\, n}\right)^{1/3} \quad , \tag{6.25}$$

corresponding to the spherical volume available to one conduction electron. In chapter 3 we had seen, that the energy per electron can be written as

$$\begin{aligned} E/N \;&=\; T \;+\; E^{\mathrm{ion-ion}} \;+\; E^{\mathrm{el-ion}} \;+\; E^{el-el} \\ &=\; T_s \;+\; E^{\mathrm{ion-ion}} \;+\; E^{\mathrm{el-ion}} \;+\; E^{\mathrm{Hartree}} \;+\; E^{\mathrm{XC}} \quad , \end{aligned} \tag{6.26}$$

where T (T_s) is the kinetic energy of the (non-interacting) electron gas, $E^{\mathrm{ion-ion}}$ and $E^{\mathrm{el-ion}}$ the energy due to ion-ion and electron-ion interaction, and the energy due to electron-electron interaction, $E^{\mathrm{el-el}}$, has been divided into Hartree and exchange-correlation contributions. For the completely smeared out constant ion density, one finds that

$$E^{\mathrm{Coulomb}} \;=\; E^{\mathrm{ion-ion}} \;+\; E^{\mathrm{el-ion}} \;+\; E^{\mathrm{Hartree}} \;=\; 0 \quad , \tag{6.27}$$

i.e. the Coulomb interaction due to the constant electron and ion densities cancels exactly. This simplifies eq. (6.26) considerably, and in the exercise you will derive that one obtains for the energy in the Hartree-Fock approximation

$$(E/N)_{\mathrm{const.\,ion}} \;=\; T_s \;+\; E^{\mathrm{XC}} \;\overset{HF}{\approx}\; \frac{30.1\,\mathrm{eV}}{\left(\frac{r_s}{a_B}\right)^2} \;-\; \frac{12.5\,\mathrm{eV}}{\left(\frac{r_s}{a_B}\right)} \quad , \tag{6.28}$$

where $a_B = 0.529\,\text{Å}$ corresponds to one Bohr. Interestingly, this energy exhibits a minimum at $r_s(o) = 4.8\,a_B$, i.e. already this crudest model of delocalized electrons leads to bonding. Before we directly proceed to analyze how this compares to the real alkalis (or how we may somewhat refine our toy model), let us first understand this quite astonishing fact. If we had treated the electron gas as independent particles, its energy would have only contained the kinetic energy T_s. As we can see from eq. (6.28), this first term is purely repulsive. Since in this approximation, the attractive electrostatic potential from the smeared-out ionic background is exactly compensated by the average repulsive field from all the other electrons, there is no reason for the electrons to stay closer together.

fcc	hcp	bcc	sc	diamond
1.79186	1.79175	1.79168	1.76012	1.67085

Table 6.7: Madelung constants for ion lattices immersed in a compensating constant electron density [from C.A. Sholl, Proc. Phys. Soc. **92**, 434 (1967)].

Adding exchange in the Hartree-Fock approximation, however, introduces the exchange-correlation hole around each electron as discussed in chapter 3. Due to this lowering of the electron density in its immediate vicinity, each electron sees now an additional attractive potential from the surrounding positive jellium background, which is not screened by the other electrons. Since the potential at the centre of a sphere of uniform charge varies inversely with the sphere radius, we expect the electron to feel an additional attractive potential proportional to $1/r_s$. This is indeed the second term in eq. (6.28), lowering the energy and leading to a binding minimum.
Having understood this, how good or bad are we actually doing with this jellium model? The alkalis crystallize in the bcc structure, which is something we cannot get out of our present model, because we have neglected the explicit form of the crystalline structure (but we will comment on the bcc structure below). The alkali atoms have one valence s electron, i.e. the number of electrons N is equal to the number of atoms M in the system. With this, we obtain for the cohesive energy

$$E^{\rm coh} \;=\; -\left(\frac{E[r_s(o)]}{M} \;-\; \frac{E[r_s\to\infty]}{M}\right) \;=\; -\frac{E[r_s(o)]}{N} \;=\; 1.3\ {\rm eV/atom} \quad . \tag{6.29}$$

And in the bcc lattice with one electron per atom, the Wigner-Seitz radius is related to the lattice constant by $a_{\rm bcc} \approx 1.1(r_s/a_B)$ (verify this!). We therefore obtain for the lattice constant $a_{\rm bcc}(o) = 5.3$ Å. Comparing these two cohesive quantities with the data compiled in Table 6.6, we are quite perplexed about the success of this admittedly trivial model.
In particular, since we are well aware that we are looking at a spitting image of reality, we should verify that this agreement is not fortuitious. First, one should check, whether the Hartree-Fock approximation does really already describe the major effect due to the electron-electron interaction. For the simple jellium system, one can fortunately calculate the correlation beyond Hartree-Fock rather well. From homogeneous electron gas theory we therefore find that such further contributions lead to a lowering of the equilibrium Wigner-Seitz radius from $r_s(o) = 4.8\,a_B$ to $r_s(o) = 4.23\,a_B$ (thus increasing the cohesive energy to 2.2 eV/atom), i.e the HF value was not too bad after all. On the other hand, the other most drastic approximation in our model was to smear out the ion lattice to a constant value. Alternatively, one can employ a lattice of point charges with $Z = e$ (for the alkalis) to resemble the atomic nuclei. Then, the Coulomb interaction of eq. (6.27) between electrons and ions does not cancel anymore. Instead one obtains (e.g. C.A. Sholl, Proc. Phys. Soc. **92**, 434 (1967))

$$E^{\rm Coulomb} \;=\; -\frac{\alpha}{2}\,\frac{e^2}{r_s} \quad , \tag{6.30}$$

where α is again a Madelung constant, containing all the information about the neighbor shells of ions in the lattice. Values for α for some lattices are given in Table 6.7. Consid-

ering the ion lattice explicitly leads therefore to another term lowering the electron energy (negative sign!), which is lowest for the lattice maximizing the Madelung constant. This lattice would correspondingly result as the stable one in our model, but looking at the values listed in Table 6.7 we find that we will be unable to distinguish between fcc, hcp and bcc lattices. That the two close-packed lattices are among the most stable is no real surprise, but the high stability of the more open bcc lattice is interesting. From the non-directionality of the metallic bond, we would have intuitively expected the close-packed lattices to be most favorable. Yet, even if this was so, our analysis shows now that the bcc lattice will be not very much less favorable (and this also results from accurate DFT calculations of the alkalis). Since entropy favors more open structures, a phase transition to bcc could therefore already occur at very low temperatures. At the finite temperatures at which experiments have been carried out to date, always the bcc structure is found for all alkali metals. Whether this is really the ground state structure, or just the result of a lowest temperature phase transition is not yet understood.
In any case, in the bcc structure the Coulomb interaction term becomes

$$E^{\text{Coulomb}} = -\frac{24.4\,\text{eV}}{\left(\frac{r_s}{a_B}\right)} \quad . \tag{6.31}$$

Adding this to eq. (6.28), we now obtain as the minimum $r_s(o) = 1.6\,a_B$, i.e. the new energy lowering term has considerably shifted the optimum for metallic binding to higher electron densities. In fact, the shift is so large, that we now obtain a way too small lattice constant of 2.7 Å, cf. Table 6.6. The reason for this overshooting in the correction compared to the smeared-out ion result is also the reason why in both cases we erroneously obtain identical lattice constants and cohesive energies for *all* alkali metals (there is no "material dependence" in the optimum electron density). Instead of point-like ions, there will in reality be a finite core region with a high density of core electrons. Due to exchange and correlation, the valence electrons will be repelled from this region and will be confined to a smaller region left in between. This increases the average electron density in this region and thus also the kinetic energy repulsion. In parallel, the valence electrons can also not come as close to the positively charged ions as in the situation approximated by the point-like lattice. This gives less negative electrostatic energy, i.e. in total both the exchange and the kinetic energy term will favor $r_s > 1.6$ (lower densities), when finite core regions are considered. Depending on the size of the core region, one will therefore describe the alkali better with either the smeared-out ion model (approximating a large core region) or with the point-like ion model (approximating a small core region). This also explains the varying cohesive values within the alkali metal series: The small core region of Li is still very well modeled by the point-like lattice model, whereas the large core region of the heavy Rb or Cs approach already the situation described better by our original smeared-out ion model.
This correspondence is in fact exploited semi-quantitatively by assigning so-called *empty-core (or Ashcroft) pseudopotentials* to each metal, such that a jellium model on the level as discussed above (but with a finite impenetrable core region corresponding to the empty-core radius) fits the experimental cohesive data (lattice constant, cohesive energy) best. Although this allows to describe quite a range of properties ranging from phonon spectra and optical absorption to superconducting transition temperatures for all simple metals, this refinement is not very instructive for our general discussion on bonding. For us, it

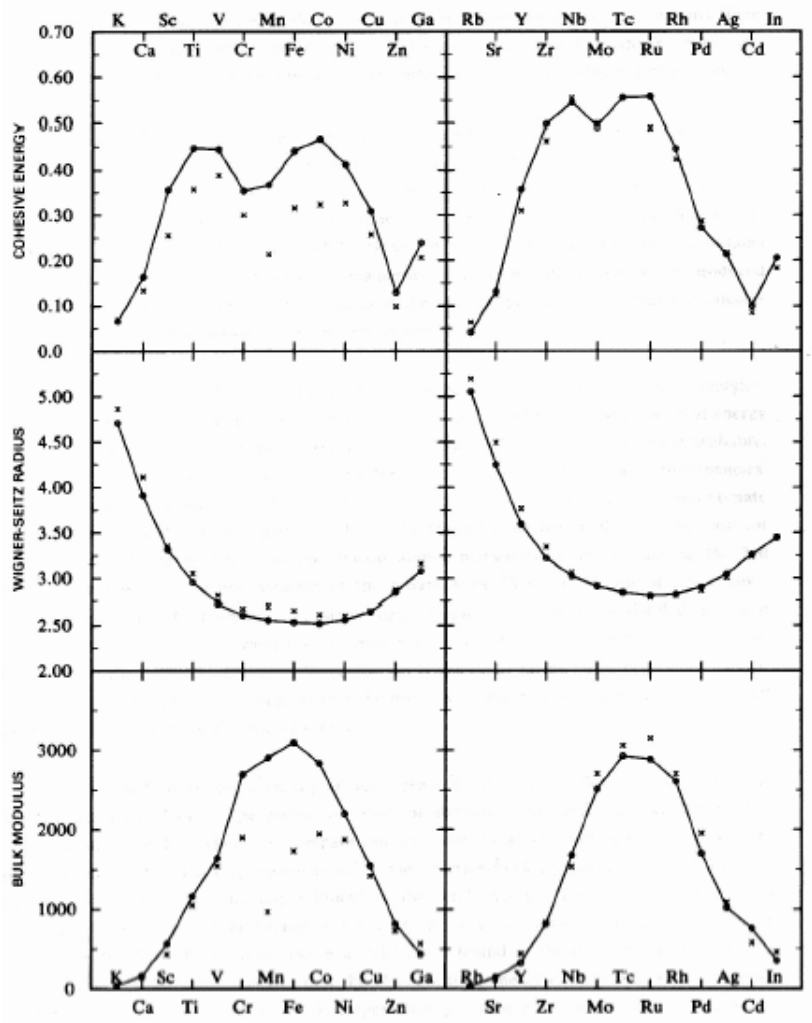

Figure 6.19: DFT-LDA (solid lines) and experimental (crosses) cohesive energies (in Ry), Wigner-Seitz radii (in a_B) and bulk moduli (in kbar) for metals of the 3rd (left) and 4th (right) rows of the Periodic Table. The calculations assume the solids to be non-magnetic and in the fcc structure. The roughly parabolic variation of the cohesive properties over one TM series is clearly visible [from V.L. Moruzzi, J.F. Janak and A.R. Williams, *Calculated electronic properties of metals*, Pergamon Press (1978)].

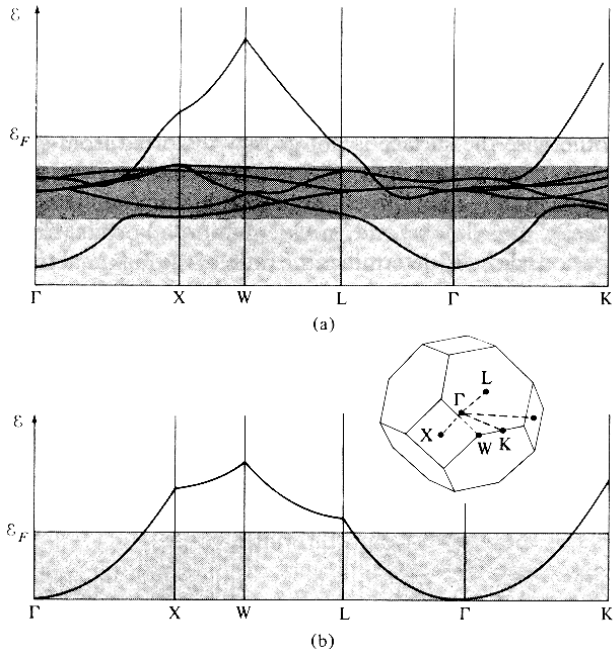

Figure 6.20: DFT-LDA band structure for Cu in the fcc structure (upper panel). The s bands are located in the region shaded in light grey and show a dispersion highly reminiscent of free electrons (the band structure of which is shown in the lower panel for comparison). In contrast, the bands deriving from the d orbitals (lying in the dark shaded region) are rather flat and have no correspondence in the free electron band structure [from Ashcroft and Mermin].

is primarily important that we understand that delocalized electrons can lead to metallic bonding. On the other hand, what we can not yet understand on the basis of our crude model (in fact not even with the refinement of empty-core pseudopotentials), is why the *transition metals* (TMs) exhibit significantly higher cohesive energies than the simple metals (W has the highest one with 8.9 eV/atom !). Furthermore, why do the cohesive properties follow roughly a parabolic pattern over one transition metal series as exemplified for the $3d$'s and $4d$'s in Fig. 6.19, which is furthermore accompanied by a systematic change of stable crystal structure from bcc over hcp to fcc when going from early to late TMs? There must be another component in the bonding responsible for this, and it is not difficult to imagine that this has to do with what is special about the TMs, namely the partly filled d valence shell.

In a general, but highly simplified view, the d-orbitals can be regarded as relatively strongly localized compared to the s valence electrons of the simple metals. A "tight-binding" type description in the sense of atomic-like orbitals is then reasonable, even in the solid. Compared to the delocalized s bands, the d bands will correspondingly be rather flat, as can indeed be seen in the band structure of Cu shown in Fig. 6.20. The valence density of states for transition metals can therefore be schematically decomposed into two contributions: a broad, featureless and essentially parabolic part due to the valence s states (comparable to the simple alkali metals) *and* a relatively narrow (few eV wide)

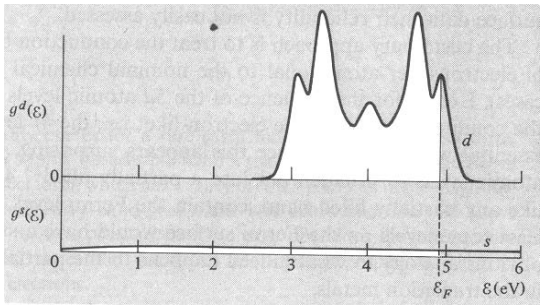

Figure 6.21: Qualitative picture of the two contributions to a TM (fcc) density of states (DOS): a wide featureless and free-electron like s band and a narrow, structured d band. Due to the larger number of d states, the d band contribution to the DOS dominates, and the varying properties over a TM series can be understood as arising from a differing degree of filling of the d band (different Fermi level position) [from Ashcroft and Mermin].

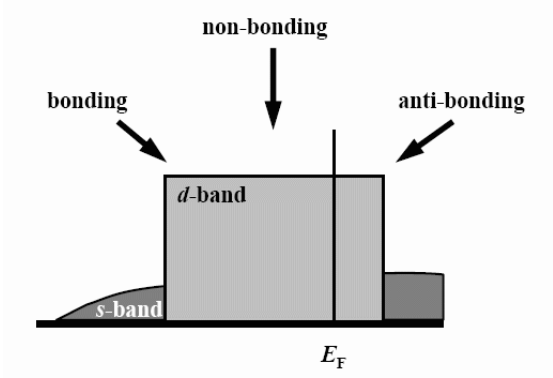

Figure 6.22: Density of states in the rectangular d band model for transition metals.

part due to the d states as illustrated in Fig. 6.21. Since there are many more d states than s states, the d contribution dominates, and the varying (cohesive) properties over a transition metal series can essentially be understood from a differing degree of filling of the d band ("rigid band model"): the number of valence electrons increases over the TM series (e.g. Ru 8, Rh 9, Pd 10, and Ag 11 valence electrons), shifting the Fermi level more and more to the right within the d band dominated DOS. At the end of a TM series, the d band is finally completely filled and the Fermi level cuts through the again s-like part of the DOS above the d band, as can e.g. be seen in the band structure of Cu shown in Fig. 6.20. Such transition metals with completely filled d bands are called *noble metals* (Cu, Ag, Au).

The simplest model reflecting this understanding of the TM valence electronic structure as a composition of nearly free electron s bands and "tight-binding" d bands is the so-called *rectangular d band model*. Here, the s states are taken as free-electron like (i.e. the jellium model discussed for the simple metals) and the d states as constant over a given band width W as explained in Fig. 6.22. Within this simple model one can analytically derive and understand surprisingly many, not only cohesive properties of TMs, and we

will encounter it again in later chapters of this lecture. Here, we content ourselves with discussing only the salient features with respect to cohesion qualitatively. Due to the more localized nature of the d orbitals, their bonding contribution is in fact more covalent than metallic. Bringing the atoms closer together results in d wave function overlap and a splitting into bonding and antibonding states yielding the narrow d band. Within this d DOS we therefore expect the lowest energy states to exhibit a more bonding character and the highest energy states to exhibit a more antibonding character. Due to the different symmetry of the d orbitals there might also be some states that cannot hybridize, which would then yield a rather non-bonding part around the center of the d band as schematized in Fig. 6.22.

What does this understanding now mean for the cohesive properties? Going over one TM series, we start with the early transition metals and accordingly begin to fill electrons into the lowest energy d states. These are of bonding type and we expect an increase in the cohesive energy. Since the DOS is dominated by d states, this rise in cohesion should be rather strong, too. Due to the shorter range of the d orbitals, their bonding contribution will also favor smaller lattice constants to maximize the wave function overlap. Towards the middle of the TM series the solids should therefore exhibit strongly increasing cohesive energies and decreasing lattice constants. The packing fraction and corresponding s electron density becomes then higher than the optimum r_s for the metallic bonding (e.g. compare the bcc lattice constants around 3 Å of the 5B and 6B TMs (V, Cr, Nb, Mo, Ta) with the $\sim$ 5 Å favored by the heavy alkalis of similar core radius!). The resulting structure and cohesion balances therefore a contractive tendency from the d orbitals with a repulsive tendency from the s electron gas (often called s *pressure*). Once the filling reaches the non-bonding and anti-bonding higher energy states in the d band (i.e. for the middle and late TMs), the increasing number of d electrons does not yield further bonding anymore, or even diminishes the existing one. The cohesive energy will level off and decrease again, while the s pressure leads to increasing lattice constants. At the noble metals, the d contribution has in this simplistic view finally canceled completely, and we reobtain cohesive properties (very roughly only!) comparable to the simple metals. Calculating through the rectangular d band model, one obtains therefore in total a parabolic shape for the cohesive energy over a TM series, and using the really computed d band widths of the order of a few eV for the parameter W, also the absolute magnitude of the cohesive energy comes out very well.

With a very crude model we can therefore (again) understand the qualitative cohesive trend over a large number of elements. What we can not reproduce with it yet, but which is something that comes out very well in state-of-the-art DFT calculations by the way, is the structural trend from bcc to hcp to fcc over the TM series and the strange dip at the top of the parabola in the middle of the TM series, cf. Fig. 6.19. The first point can obviously not be understood within the rectangular d band model, since there is no explicit lattice structure contained in it. When one considers the latter, say in DFT calculations, one finds that the lattice affects the sub structure within the d DOS that is apparent in Fig. 6.21, but neglected in the coarse rectangular d band model. One can understand this sub structure in the DOS directly from the band structure: The DOS results from the integration over the Brillouin zone; points that occur often and where the bands are relatively flat, will thus give rise to a high density of states. For the fcc lattice, cf. Fig. 6.21, one would for example typically expect five peaks, three associated with the (eightfold occurring) L point and two with the (sixfold occurring) X point, cf.

Fig. 6.20. The shape of the d DOS is in other words quite characteristic for a given lattice type, not so much for the element (which more dictates the *filling* of the d DOS, again in the view of the "rigid band model"). Comparing this characteristic shape for bcc, hcp and fcc structures one can discern e.g. a rather skewed form of the bcc d DOS with many low lying states. All three lattices (bcc, fcc, hcp) offer almost the same volume per atom, in which case one can show that the contribution from the single particle energies governs the final total energy [H.L. Skriver, Phys. Rev. B **31**, 1909 (1985)]. If a particular lattice structure offers therefore an optimum number of bonding states for a given filling fraction (like the bcc structure for small fillings), it will result as most stable. With the characteristic DOS shapes, we therefore obtain in all three TM rows the same sequence bcc $\rightarrow$ hcp $\rightarrow$ fcc depending on the filling ratio (a more in depth discussion of this point can for example be found in D. Pettifor, *Bonding and Structure of Molecules and Solids*, Clarendon Press (1995)).

This leaves as the last point the dip in the middle of the TM series, cf. Fig. 6.19, as well as the rather annoying quantitative discrepancy between the DFT and experimental data for the $3d$ row (up to 20-50 %). The reason behind the first point are special atomic properties (remember that the cohesive energy results as the difference between the energy of the isolated atom and the solid!). In the middle of the TM series, i.e. for Mn ($3d^5 4s^2$) and Mo ($4d^5 5s^1$), the $d-d$ correlation is particularly important and leads to a pronounced stability of the isolated atom. In the solid this is less important, i.e. there is no unusual stability compared to the overall TM trend, yielding in total a diminished cohesive energy for these elements and a dip in the parabola. The quantitative difference for the $3d$ row, on the other hand, is primarily due to the fact that the (older) calculations of Moruzzi, Janak and Williams did not consider magnetic effects (non-spin polarized calculations). This aspect is, however, very important for the $3d$'s with their strong localization, and we will come back to this point in the chapter on magnetism. In any case (even with state-of-the-art spin polarized calculations), for the cohesive energy we need (unfortunately) also atomic calculations. Due to the strong localization of the $3d$ orbitals, such calculations are essentially problematic for DFT-LDA or DFT-GGA, leaving still an unsatisfying disagreement for the $3d$ TM solids.